Thin Solid Films 529 (2013) 263–268

Contents lists available at SciVerse ScienceDirect

Thin Solid Films

journal homepage: www.elsevier.com/locate/tsf

Nonvolatile floating gate memory characteristics of Sb_2Te–SiO_2 nanocomposite thin films

Cheng-Hsun Yang, Kuo-Chang Chiang, Tsung-Eong Hsieh *

Department of Materials Science and Engineering, National Chiao Tung University, 1001 Ta-Hsueh Road, Hsinchu 30010, Taiwan, ROC

ARTICLE INFO

Available online 17 September 2012

Keywords:
Chalcogenides
Sb_2Te
Nanocomposite
Nonvolatile floating gate memory

ABSTRACT

Nonvolatile floating gate memory (NFGM) device composed of Sb_2Te nanocrystals (NCs) as the charge-storage traps embedded in SiO_2 matrix was prepared by the target-attachment sputtering method at various nitrogen (N_2) incorporation conditions. *Via* post annealing at 450 °C in ambient air, the sample prepared at the condition $N_2/Ar = 0.1$ exhibited a maximum memory window (ΔV_{FB}) shift = 4.4 V and charge density = 4.2×10^{12} cm^{-2} under ±7 V gate voltage sweep. N_2 incorporation not only reduced the Sb_2Te NC size to about 5 nm, but also suppressed the oxygen defects and antimony oxides in the sample. Feasibility of the Sb_2Te chalcogenide NCs to NFGM fabrication with the simplified process and relatively low annealing temperature is demonstrated.

1. Introduction

Nonvolatile floating gate memory (NFGM) is a key component to the portable electronic products in the present day. However, the conventional NFGM suffers high leakage current and poor reliability due to the scale-down limitation [1,2]. The device composed of discrete nanocrystals (NCs) as the charge storage traps embedded in dielectric matrix is hence proposed to replace the memory device with continuous layer structure. It offers the advantages including low power consumption, fast write/erase speed, small voltage operation and high endurance [1–3]. The NFGM containing Si NCs embedded in a SiO_2 matrix was first proposed by Tiwari et al. [1]. Since then, various transition metal NCs, *e.g.*, cobalt (Co) [4], ruthenium (Ru) [5], platinum (Pt) [6], and iridium (Ir) [7] have been implanted in the NFGMs due to their advantages of high thermal stability, wide range of work function, and large density of states around Fermi level. Presently, a memory window (ΔV_{FB}) shift = 17.4 V with charge density = 1.17×10^{13} cm^{-2} under −15 V to +13 V gate voltage sweep was achieved in NFGM containing Ir NCs [7]. However, several difficulties remain to be overcome for the metallic NC-based NFGMs, for instance, the metal interdiffusion and oxidization during high-temperature annealing (usually above 600 °C) might degrade the memory performance [4–7]. Moreover, complicated fabrication methods are frequently required in order to gain control on the thickness and quality of oxide layer presenting in between the dielectric layer and the Si substrate [8]. In order to reduce leakage current and improve thermal stability, nitrogen (N_2) incorporation has been adopted to eliminate the undesired features brought by the oxide interfacial layer due to its strong coupling with oxygen vacancies [9].

Chalcogenides are well-known phase-change recording media for optical data storage [10]. They possess ultra fast recrystallization rates and comparatively low recrystallization temperatures and, hence, it is the purpose of this work to explore the feasibility of chalcogenide NCs to NFGM so as to achieve a simple fabrication method in conjunction with low-temperature annealing process. Nucleation-dominated chalcogenide, $Ge_2Sb_2Te_5$ [11] and doped growth-dominated chalcogenide, AgInSbTe [12], in NC form have been demonstrated to possess a significant NFGM property. Sb_2Te possesses a high work function (4.61 eV) [13,14] that may generate a deep trap for charge storage. Nevertheless, the NFGM study regarding of the dopant-free growth-dominated alloy, Sb_2Te, is still missing. This study prepares the Sb_2Te–SiO_2 nanocomposite thin films by the target-attachment sputtering method [12] at various N_2 incorporation conditions. The memory performance of NFGM containing such nanocomposite layers is evaluated and its correlations to the microstructure and chemical status of elements are discussed in the following.

2. Experimental details

A Metal-insulator-semiconductor (MIS) capacitor containing Sb_2Te–SiO_2 nanocomposite layer was deposited on *p*-type, Si (100) substrates (resistivity = 1–10 Ω·cm). A schematic illustration of the device structure is shown in Fig. 1. Prior to the deposition, all Si substrates were cleaned by standard RCA process and soaked in a diluted hydrofluoric acid solution to remove the native oxides. Afterward, 25-nm thick Sb_2Te–SiO_2 nanocomposite layers were deposited on the Si substrate by target-attachment method in a sputtering system with a background pressure better than 2.7×10^{-4} Pa. The Sb_2Te pellets in disc form with 12 mm in diameter and 1.5 mm in thickness were first prepared by pressing the Sb_2Te powder in the mold at a pressure of 100 MPa. Appropriate amount of Sb_2Te pellets was then attached on

* Corresponding author. Tel.: +886 3 5712121x55306; fax: +886 3 5724727.
E-mail address: tehsieh@mail.nctu.edu.tw (T.-E. Hsieh).

0040-6090/$ – see front matter © 2012 Elsevier B.V. All rights reserved.
http://dx.doi.org/10.1016/j.tsf.2012.07.135

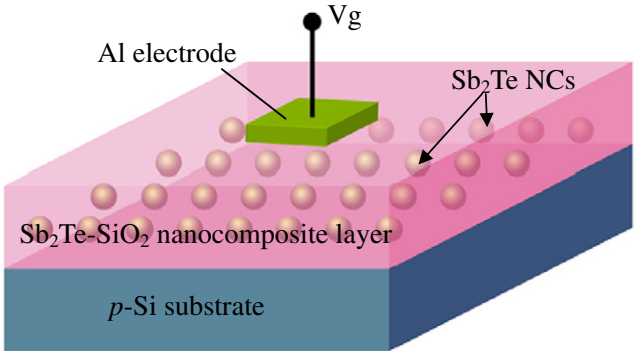

Fig. 1. Schematic illustration of NFGM device structure.

the 3-inch quartz target for subsequent sputtering deposition of nanocomposite layers. Since the content of Sb_2Te NCs in nanocomposite layer is proportional to the number of Sb_2Te pellets, one could thus adjust the density of charge trapping sites in NFGM sample to achieve the desired electrical performance. As mentioned above, complicated methods such as atomic layer deposition were often required to prepare the blocking oxide/NCs/tunneling oxide device structure for NC-based NFGMs [15]. Analytical results presented in the following illustrate that such a multilayer device structure can be achieved in the chalcogenide NC-based nanocomposite layers prepared by the target-attachment method. It is hence a simple and versatile thin-film deposition process which allows us to verify the feasibility of chalcogenides to NFGM fabrication.

In this work, the deposition was carried out without intentional substrate heating at radio-frequency sputtering power of 80 W, working pressure of 0.4 Pa and various Ar/N_2 inlet gas flow ratios (in the unit of sccm) of 10:0 (N_{00} sample), 10:1 (N_{10} sample) and 10:2 (N_{20} sample). The N_{00}, N_{10} and N_{20} samples were deposited at the rates of 1.9, 0.6 and 0.5 nm/min, separately, and the thickness of the nanocomposite layers was fixed at 25 nm. N_2 addition is known to eliminate the oxygen defects and reduce the leakage current of dielectric layers [16]. Effects of N_2 content on the interfacial states at the NC/oxide interfaces and the charge trapping properties of NC-based NFGMs have been reported previously [17]. Moreover, the studies of phase-change media for optical discs found that the recrystallization behaviors of chalcogenides can be modulated by N_2 doping [18]. Since the effect of N_2 incorporation on the chalcogenide NC-based NFGM is not fully understood, this study hence varies the Ar/N_2 inlet gas flow ratios during sputtering so as to investigate its influence on the microstructure of Sb_2Te–SiO_2 nanocomposite layers and the performance of NFGM. Subsequently, the post annealing at 450 °C for 270 s in ambient air was performed in order to induce the recrystallization of Sb_2Te phase in nanocomposite layers. Note that the annealing condition has been optimized to achieve the best memory performance. Finally, 300-nm thick Al electrodes with 0.2 mm in diameter were deposited by *e*-beam evaporation to complete the sample preparation.

The microstructures of NFGM devices were characterized by transmission electron microscopy (TEM, FEI TECNAI G2 F20 S-TWIN) with an operating voltage of 200 kV. The cross-sectional TEM (XTEM) samples were prepared by the focused ion beam (FIB, FEI Helios 400S) technique using the 8-keV Ga^+ ion source for sample milling. An energy dispersive spectroscopy (EDX, Link ISIS 300) attached to the TEM was adopted to analyze the stoichiometric ratio of chalcogenide NCs. The chemical status of the elements in nanocomposite samples was analyzed by an X-ray photoelectron spectroscopy (XPS, PHI Quantera SXM) using monochromic Al K_α (1486.6 eV) radiation as the X-ray source. The curve fitting of XPS profiles was achieved by using the XPS Peak 4.1 software. The spectra were de-convoluted with a Shirley background and optimized by allowing the 100% Gaussian with fixed full width at half maximum. Capacitance–voltage (*C*–*V*) and charge retention properties of NFGM devices were evaluated by a HP 4284A precision LCR meter at a frequency of 1 MHz. Current–voltage (*I*–*V*) measurement was carried out by using an HP 4156B semiconductor parameter analyzer in conjunction with a probe tester (SANWA, WM-365A-1). All electrical measurements were performed in ambient air at room temperature.

3. Results and discussion

Fig. 2(a) presents the *C*–*V* characteristics of various NFGM samples subjected to ±7 V gate voltage sweeps. It is worthy to note that the counterclockwise hysteresis loops indicate electron trapping/detrapping in NCs during the substrate injection [3]. The N_{00} sample exhibits a negligible ΔV_{FB} shift of 0.4 V, indicating the poor charge storage in NCs during the memory operation. As to N_{10} and N_{20} samples, the ΔV_{FB} shifts of 4.41 V and 3.38 V with the corresponding charge densities of 4.21×10^{12} cm^{-2} and 3.61×10^{12} cm^{-2} were achieved. Moreover, the significant negative shifts of *C*–*V* profiles imply the presence of positive fixed charges, *e.g.*, oxygen vacancies, in nanocomposite layer [19]. Though the *C*–*V* results shown in Fig. 2(a) clearly indicate that N_2 incorporation enhances the charge storage capability of NCs, excessive N_2 addition in fact degrades the electrical performance as revealed by the *C*–*V* profile of N_{20} sample. This is ascribed to the formation of nitrides near the substrate which would trap the charges and suppress the Coulomb's blockage effect in the nanocomposite layer [20]. The presence of nitride phase in the samples will be discussed in the following XPS analysis.

Fig. 2(b) presents the current density–electrical field (*J*–*E*) characteristics of the samples deduced by the *I*–*V* measurement. At the substrate injection case (*i.e.*, positive bias on the top Al electrode), N_{10} sample apparently exhibits the lowest leakage current density of 1.28×10^{-10} A/cm^2 at a bias field of 8 MV/cm in comparison with the other samples. This implies a good Coulomb's blockage effect on such sample that the suppression of charge de-trapping from NCs to the substrate would benefit the data retention property [21]. In the case of gate injection (*i.e.*, negative bias on the top Al electrode), relatively high leakage currents were observed for all samples. This indicates a preference of charge injection from NCs to the gate electrode. Lee et al. pointed out that the asymmetric *J*–*E* behavior of memory device is resulted from the difference in energy barrier height for charge transport [22]. Fig. 2(c) presents the schematic band diagram of NFGM samples at the substrate and gate injection cases. Notably, the presence of the ultrathin TeO_2 and SiO_2 layers in NFGM sample will be illustrated by the following TEM and XPS characterizations. In the case of substrate injection, the electrons have to tunnel through the SiO_2 layer with a relatively high barrier (E_g = 9 eV) to the nanocomposite layer so as to be trapped in Sb_2Te NCs. On the other hand, electrons tunnel from gate electrode through the TeO_2 layer with low barrier height (E_g = 3.75 eV) [23] in the case of gate injection. The low energy barrier height feature of TeO_2 would result in a large tunneling current. This also implies that the charges stored in NCs may jump back to the gate electrode due to the low energy barrier. This consequently degrades the trapping efficiency and a high leakage current in gate injection case.

Table 1 summarizes the charge retention characteristics of NFGM samples. The retention was measured by a voltage stress of ±5 V on the top Al electrode in 10 s interval. Notably, the retention properties of the N_{00} sample diminished at about 10^3 s. The best retention property was observed in N_{10} sample which exhibits the ΔV_{FB} shift of 2.05 V and the charge loss of 27.8% after the test duration for 10^4 s. The electrical characterizations clearly indicated that appropriate N_2 incorporation improved the charge retention property of NFGM, indicating a result of imperfection remedy in the nanocomposite layer revealed by the following microstructure and composition analyses. Electrical analyses presented above also illustrate the feasibility of Sb_2Te–SiO_2 nanocomposite layer to NFGM fabrication. *Via* a one-step sputtering process, the single programming-layer memory device

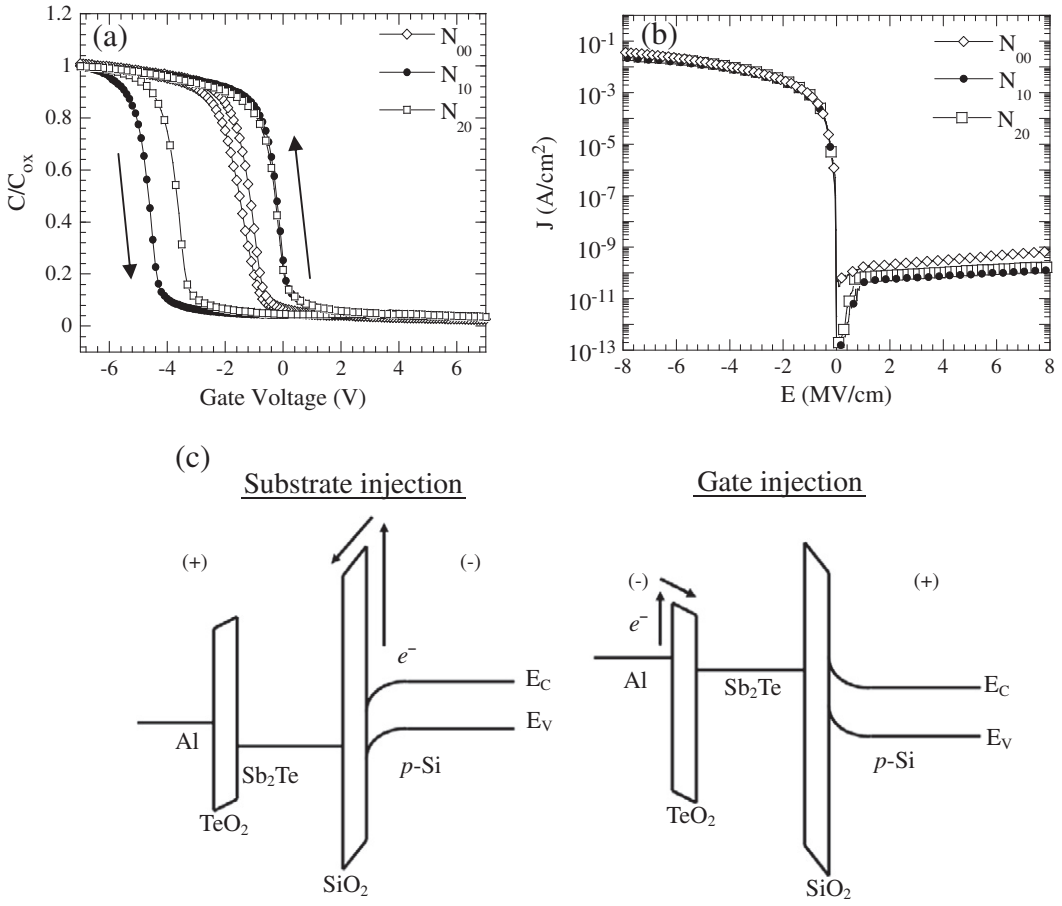

Fig. 2. (a) *C–V* and (b) *J–E* characteristics of NFGM samples. The gate voltage sweep range is ±7 V for *C–V* measurement. (c) Schematic energy band diagrams of NFGM samples under substrate and gate injection processes.

with satisfactory electrical performance can be achieved. Moreover, it effectively saves the thermal budget of the NFGM process since the utilization of chalcogenide NCs as the charge traps dramatically reduces the temperature and time span of post annealing process in comparison with previous studies [4–7].

XTEM images of Sb_2Te–SiO_2 nanocomposite layers in the N_{00}, N_{10} and N_{20} samples are separately presented in Fig. 3(a)–(c). It can be readily seen that the amount of N_2 incorporation affects the sizes and distribution of Sb_2Te NCs in the nanocomposite layer. As shown in Fig. 3(a), the column-like Sb_2Te phase emerges in the N_{00} sample. Severe overlapping of Sb_2Te NCs occurred in such a sample that it not only impoverishes the charge trap sites, but also forms the leakage channel of charges. This explains the poor *C–V* performance of N_{00} sample as depicted in Fig. 2(a). Uniformly dispersed Sb_2Te NCs with size of about 5 nm were observed in N_{10} sample as shown in Fig. 3(b) and (d). This illustrates that appropriate N_2 incorporation may result in the discrete NCs and hence suppresses the lateral charge loss [21]. Moreover, it increases the number of NCs and, hence, the number of charge trapping sites in the nanocomposite layer. A satisfactory memory performance was thus achieved in the N_{10} sample. As to N_{20} sample, it contains ultra small Sb_2Te NCs with size of about 3–4 nm as shown in Fig. 3(c). Though the number of NCs seemed to increase with increasing N_2 incorporation, TEM characterization revealed rather weak and vague image contrast for NCs in N_{20} sample. This implies a suppression of crystallinity of chalcogenide phase due to excessive N_2 addition. The studies relating phase-change media for optical discs reported that the N_2 doping results in the formation of nitride phases which may alter the recrystallization behaviors of chalcogenides [18]. As a matter of fact, the following XPS analysis reveals the presence of antimony nitride (Sb_3N_4) in the N_2-incorporated samples. The NCs with ultra small size and poor crystallinity hence formed in the N_{20} sample. Moreover, excessive N_2 incorporation during sputtering is known to amplify the chemical etching effect of the deposited layer. This also degrades the quality of nanocomposite layer and, hence, the memory performance of N_{20} sample.

We note that EDX analysis performed in the TEM indicates the stoichiometric ratio of chalcogenide NCs is Sb:Te = 2:3 for all samples. The study on Sb_2Te found that its structure can be viewed as a sequential stacking of Sb_2Te_3 and Sb_2 layers [24]. It is inferred that the Sb portion of Sb_2Te might react with oxide matrix to form the antimony oxide on the NC surfaces while the Sb_2Te_3 portion becomes the dominant constitution of NCs. Evolution of such a metal oxide will be discussed in the subsequent XPS analysis. Moreover, the TEM micrographs shown in Fig. 3 revealed, regardless of N_2 incorporation, a SiO_x layer with thickness of about 3–5 nm is present at the nanocomposite/Si interface in all samples.

Table 1
Summary of charge retention characteristics of NFGM samples.

Sample designation	ΔV_{FB} shift (after 10^4 s retention)	Charge loss (at ±5 V)
N00[a]	–	–
N10	2.05 V	27.8%
N20	2.03 V	28.9%

[a] Memory property diminished in less than 10^3 s.

Such a thin SiO_x interfacial layer can be clearly seen in the enlarged micrograph shown in Fig. 3(d). It not only serves as the tunneling layer for charge transport, but also provides an effective barrier for charge storage in the nanocomposite layer.

Fig. 4(a)–(d) depict the XPS spectra and the corresponding deconvoluted profiles obtained by the Gaussian fitting method [25]. Prior to the XPS analysis, removal of about 20-nm thick nanocomposite layer was performed by 1-keV/20-mA Ar^+ ion sputtering in *in-situ* manner to expose the region enriched with chalcogenide NCs. Fig. 4(a) presents the N 1*s* XPS spectra of N_{10} and N_{20} samples in which the curve fitting of the spectra reveals the presence of Si–N (398.2 eV) and Sb–N (401.8 eV) bonds in the N_2-incorporated samples. This indicates that N_2 incorporation during sputtering may result in the nitride phases, *e.g.*, Si_3N_4 and Sb_3N_4, in the nanocomposite layers. It is noted that the corresponding XPS peak intensities are rather weak, indicating the small nitride contents in the samples due to the low N_2 inlet gas flow adopted for sample preparation. As shown by Si 2*p* XPS spectra in Fig. 4(b), a relatively high intensity of suboxide phase, *i.e.*, SiO_x (102.4 eV), in the N_{00} sample implies the abundance of oxygen defects in such sample. As to the N_{10} and N_{20} samples, the dominance of the SiO_2 (103.3 eV) component indicates that N_2 incorporation suppresses the oxygen defects in the nanocomposite layers. The increase of SiO_2 peak also indicates that a dense oxide component is built in the nanocomposite layer, implying the lower leakage and better charge retention properties of N_{10} and N_{20} samples as depicted in Fig. 2(a) and (b). In addition, a small amount of silicon nitride (Si_3N_4; 101.8 eV) emerging in Fig. 4(b) also manifested the presence of Si–N bonds in the matrix of nanocomposite layer. It is plausible that a portion of SiO_2 may transform into the oxide–nitride mixtures, *e.g.*, SiO_xN_y, which are known to suppress the charge hopping process and improve the leakage property of the samples [26].

The Sb 3*d* XPS spectra shown in Fig. 4(c) reveal the Sb_2O_3 phase (530 eV in $3d_{5/2}$ region; 539.6 eV in $3d_{3/2}$ region) in the N_{00} sample. The antimony oxide likely resulted from the oxidization of NCs during the annealing at 450 °C in ambient air by interacting with oxide matrix *via* the reactions $3Sb_2Te + 3SiO_2 \rightarrow Sb_2(Si,Te)_3 + 2Sb_2O_3$. This also explains the detection of a Sb_2Te_3 phase in the samples by EDX analysis. As to the N_{10} and N_{20} samples, Fig. 4(c) indicates that N_2 incorporation effectively eliminates the Sb_2O_3 phase and results in the small amount of Sb_3N_4 phase (530.2 eV in $3d_{5/2}$ region; 539.6 eV in $3d_{3/2}$ regions) in the nanocomposite layers. The removal of Sb_2O_3 component in the N_{10} and N_{20} samples suggests that the suppression of antimony oxide by appropriate N_2 incorporation benefits the memory performance.

Te $3d_{5/2}$ XPS spectra for all samples are presented in Fig. 4(d). It can be readily seen that the N_2 incorporation and post annealing conditions do not affect the chemical status of Te in the interior of the nanocomposite layer which remains in a form of metallic Te (572.85 eV). Nevertheless, the Te $3d_{5/2}$ XPS depth profile of N_{10} sample shown in Fig. 5 reveals a 3-nm thick TeO_2 layer residing on the nanocomposite surface. The thin TeO_2 layer was similarly observed in other samples and it is noted that, once the nanocomposite samples were removed from the vacuum chamber, such TeO_2 surface layer inevitably formed on the samples as revealed by the composition analysis. This indicates that the reaction of chalcogenide with oxygen in ambient air is most likely the cause of TeO_2 formation. Once it formed on the sample surface, the TeO_2 seemed to passivate the nanocomposite layer since no Te oxidization further occurred in the interior of the nanocomposite layer as revealed in Figs. 4(d) and 5. Similar to the SiO_2 layer at the nanocomposite/Si substrate interface, the TeO_2 layer at the nanocomposite/Al electrode interface might serve as a tunneling layer for charge transport and the charge confinement layer in NFGM

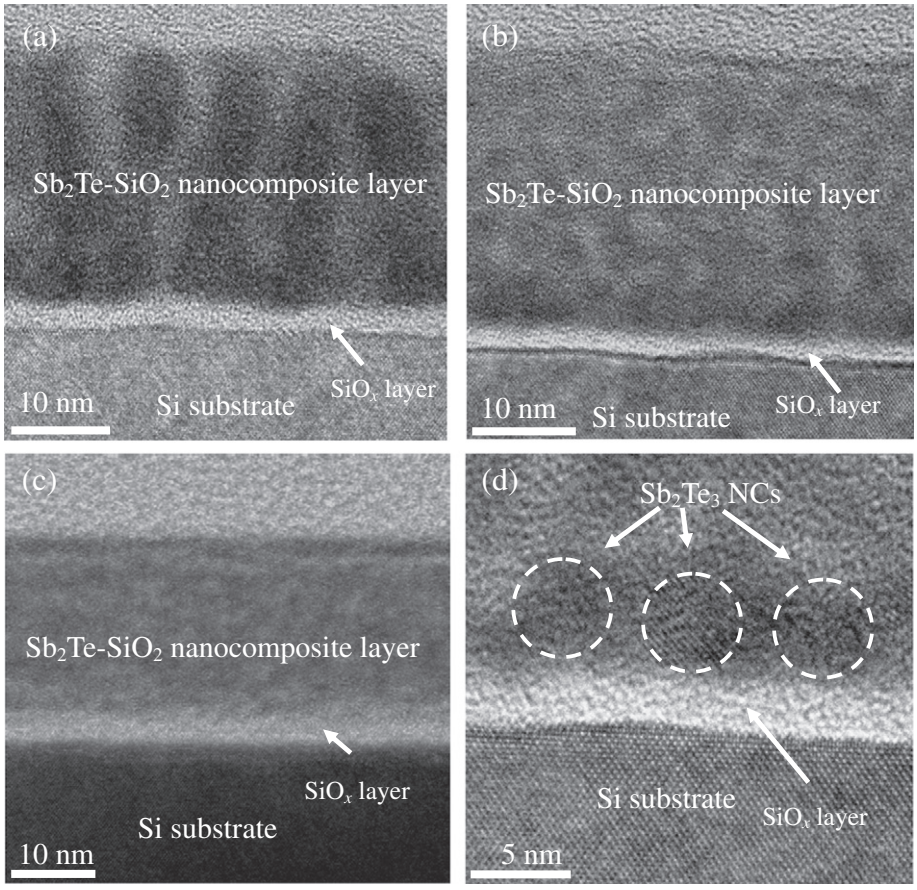

Fig. 3. XTEM micrographs of (a) N_{00}, (b) N_{10} and (c) N_{20} samples. Enlarged micrograph shown in (d) is taken from N_{10} sample at the nanocomposite layer/Si substrate interface.

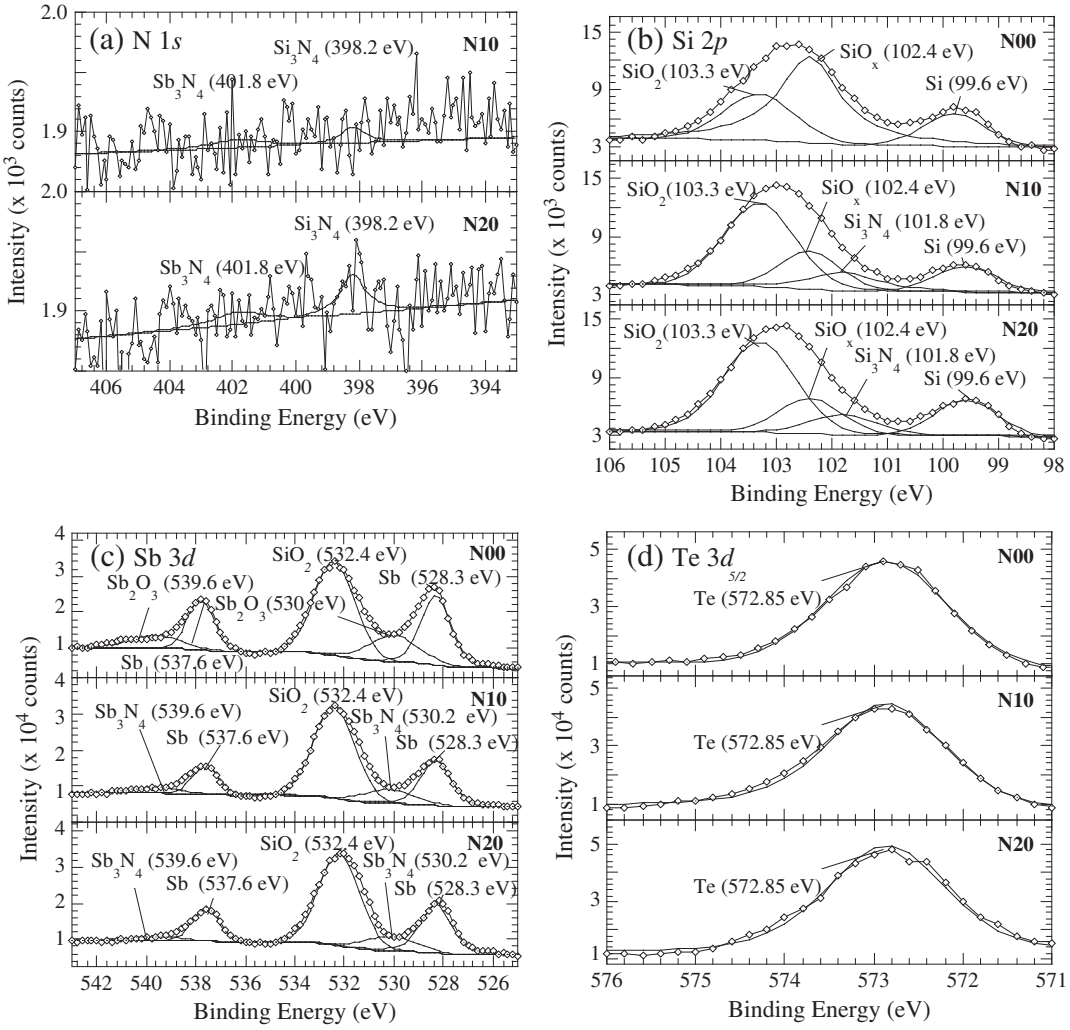

Fig. 4. (a) N 1*s*, (b) Si 2*p*, (c) Sb 3*d* and (d) Te $3d_{5/2}$ XPS spectra for nanocomposite samples prepared at various N_2 incorporation conditions. The solid black curves with open diamond symbols correspond to raw XPS data while the black curves are the profiles obtained by Gaussian fitting.

device containing chalcogenide NCs. However, TeO_2 is not effective as a barrier compared to the SiO_2 layer due to its lower barrier height as mentioned previously.

4. Conclusions

Chalcogenide NCs serving as the charge traps were implanted in the NFGM devices by using the target-attachment sputtering method. With a supply of Ar/N_2 inlet gas flow at the ratio of 10:1 during the sputtering deposition, a significant ΔV_{FB} shift = 4.41 V and charge density = 4.21×10^{12} cm^{-2} at ±7 V gate voltage sweep were achieved in the NFGM sample. Moreover, the ΔV_{FB} shift about 2.05 V and the charge loss about 27.8% were observed after10^4s retention test at ±5 V gate voltage stress. Analytic results indicated that appropriate N_2 incorporation may not only suppress the number of oxygen defects, but also eliminate the formation of antimony oxides in the nanocomposite layer. This promoted the charge storage capacity and yielded a significant memory performance in NFGM device. This study demonstrated that a single chalcogenide NCs–SiO_2 nanocomposite is feasible as the programming layer of NFGM device. In addition to the simplification of device fabrication, utilization of chalcogenide NCs may also save the thermal budget in an effective manner and is a promising alternative for advanced NFGM fabrication in the future.

Acknowledgments

The study is supported by the National Science Council (NSC), Taiwan, ROC, under the contract no. NSC100-2221-E-009-054-MY2. TEM and XPS analyses supported by the Materials Analysis Technology Inc. at Jubei,

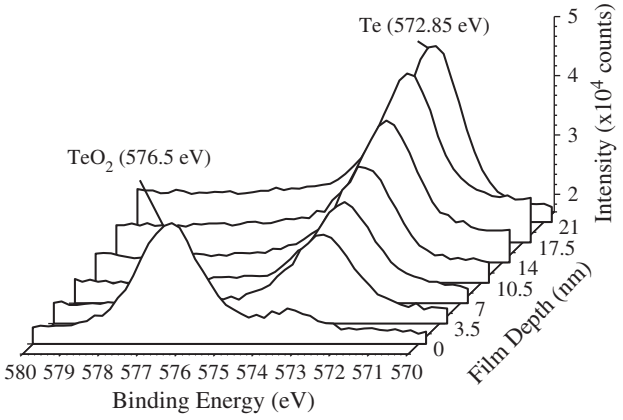

Fig. 5. Te $3d_{5/2}$ XPS depth profiles for N_{10} sample.

Taiwan, ROC, and the Instrument Center at National Tsing Hua University at Hsinchu, Taiwan, ROC, are also deeply acknowledged.

References

[1] S. Tiwari, F. Rana, H. Hanafi, A. Hartstein, E.F. Crabbe, K. Chan, Appl. Phys. Lett. 68 (1996) 1377.
[2] T.H. Ng, V. Ho, L.W. Teo, M.S. Tay, B.H. Koh, W.K. Chim, W.K. Choi, A.Y. Du, C.H. Tung, Thin Solid Films 462 (2004) 46.
[3] C.L. Yuan, P. Darmawan, Y. Setiawan, P.S. Lee, J. Ma, Appl. Phys. Lett. 89 (2006) 043104.
[4] B. Li, J. Liu, Appl. Phys. Lett. 91 (2007) 052905.
[5] D.B. Farmer, R.G. Gordon, J. Appl. Phys. 101 (2007) 124503.
[6] S. Novak, B. Lee, X. Yang, V. Misra, J. Electrochem. Soc. 157 (2010) H589.
[7] T.T.-J. Wang, C.-L. Chu, I.-J. Hsieh, W.-S. Tseng, Appl. Phys. Lett. 97 (2010) 143507.
[8] H.X. Xu, J.P. Xu, C.X. Li, P.T. Lai, Appl. Phys. Lett. 97 (2010) 022903.
[9] X.J. Wang, L.D. Zhang, M. Liu, J.P. Zhang, G. He, Appl. Phys. Lett. 92 (2008) 122901.
[10] C.C. Chou, F.Y. Hung, T.S. Lui, Scr. Mater. 56 (2007) 1107.
[11] T. Eom, B.J. Choi, S. Choi, T.J. Park, J.H. Kim, M. Seo, S.H. Rha, C.S. Hwang, Electrochem. Solid-State Lett. 12 (2009) H378.
[12] K.-C. Chiang, T.-H. Hsieh, Nanotechnology 21 (2010) 425204.
[13] K.I. Grais, A.M. Bastaweos, J. Appl. Phys. 53 (1982) 5239.
[14] Y.M. Zuev, J.S. Lee, C. Galloy, H. Park, P. Kim, Nano Lett. 10 (2010) 3037.
[15] Y.-S. Lo, K.-C. Liu, J.-Y. Wu, C.-H. Hou, T.-B. Wu, Appl. Phys. Lett. 93 (2008) 132907.
[16] T.-M. Pan, S.-J. Hou, C.-H. Wang, J. Appl. Phys. 103 (2008) 124105.
[17] Z. Tan, S.K. Samanta, W.J. Yoo, S. Lee, Appl. Phys. Lett. 86 (2005) 013107.
[18] R. Kojima, S. Okabayashi, T. Kashihara, K. Horai, T. Matsunaga, E. Ohno, N. Yamada, T. Ohta, Jpn. J. Appl. Phys. 37 (1998) 2098.
[19] K.K.S. Curreem, P.F. Lee, K.S. Wong, J.Y. Dai, M.J. Zhou, J. Wang, Q. Li, Appl. Phys. Lett. 88 (2006) 182905.
[20] W.R. Chen, T.C. Chang, J.L. Yeh, S.M. Sze, C.Y. Chang, Appl. Phys. Lett. 92 (2008) 152114.
[21] J.J. Lee, D.-L. Kwong, IEEE Trans. Electron Devices 52 (2005) 507.
[22] D.-J. Lee, S.-S. Yim, K.-S. Kim, S.-H. Kim, K.-B. Kim, J. Appl. Phys. 107 (2010) 013707.
[23] K. Arshak, O. Korostynska, Sensors 2 (2002) 347.
[24] V. Agafonov, N. Rodier, R. Ceolin, R. Bellissent, C. Rergman, J.P. Gaspard, Acta Crystallogr. C47 (1991) 1141.
[25] J.F. Moulder, W.F. Stickle, P.E. Sobol, K.D. Bombem, Handbook of X-ray Photoelectron Spectroscopy, 2nd ed. Physical Electronics, Minnesota, 1992.
[26] Y.-Y. Peng, T.-H. Hsieh, C.-H. Hsu, J. Nanosci. Nanotechnol. 9 (2009) 4892.